Supplementary Information for "Frequency dependence of seismic attenuation and coupling through Mars' regolith: implications for the InSight Mission"

Myhill et al.

May 17, 2018

S1 Coherence between seismometer recordings in active source experiments

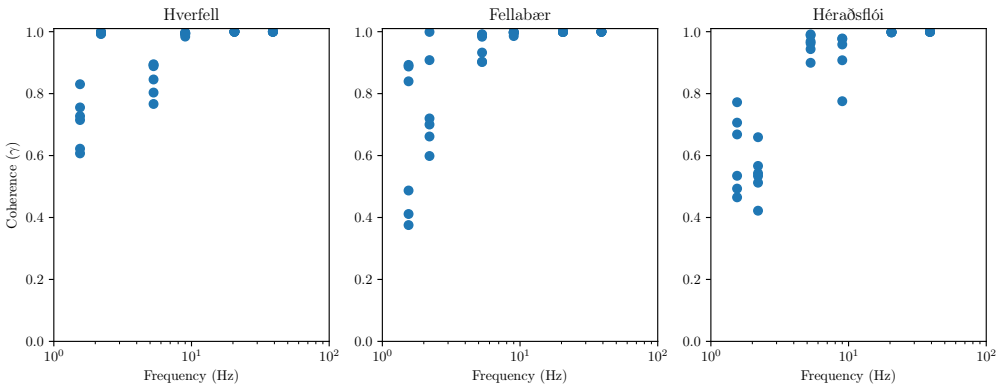

Figure S1: Magnitude of the coherence between the inner and outer tripod-mounted seismometers for the experiments described in Section 5.1 of the main manuscript (and in Figure 7). The coherence is very high at high frequencies, and drops significantly only at the lowest frequencies.

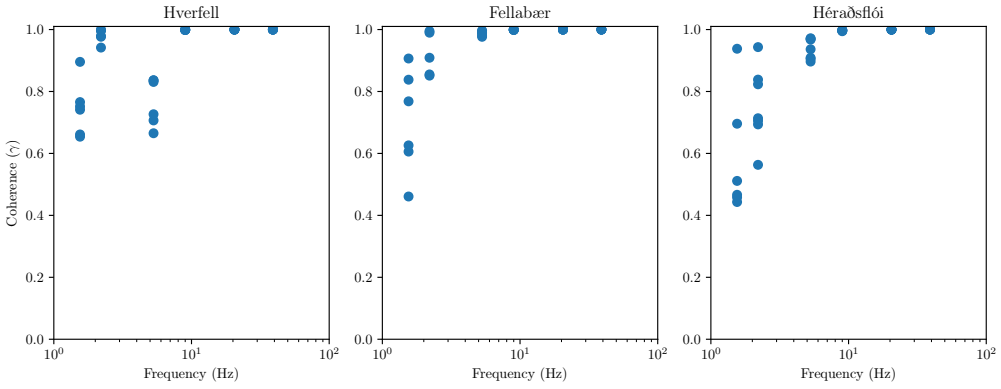

Figure S2: Magnitude of the coherence between the tripod-mounted seismometer and buried seismometer for the spring-source experiments described in Section 5.2 of the main manuscript (and in Figure 10). The coherence behaviour is similar to that in Figure S1.

S2 Noise response

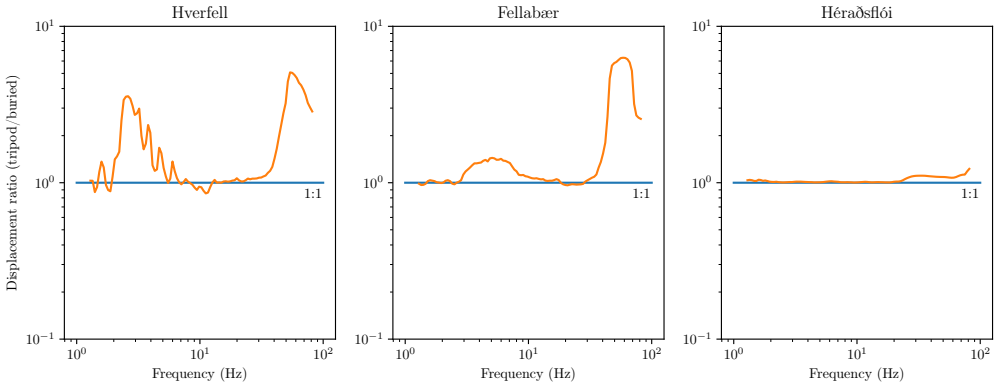

Figure S3: Amplitude of vertical displacement of the tripod-mounted seismometer driven by ambient noise, normalised by the displacement of a seismometer buried directly underneath the tripod. This figure corresponds to the ambient noise experiments described in Section 5.2 of the main manuscript (and in Figure 9).

S3 Finite element modelling

We use the finite-element software FEniCS (Logg et al., 2012; Alnæs et al., 2015) to model the elastic deformation of a regolith with a Young's modulus profile of the form:

$$E = A\left(b + \frac{z}{r_f}\right)^k \tag{1}$$

$$A = E_r\left(\frac{\rho g r_f}{\sigma_r}\right)^k \tag{2}$$

$$b = \frac{\sigma_{c0}}{\rho g r_f} \tag{3}$$

The variational form of the elasticity problem (neglecting the body forces due to gravity) is:

$$\int_V \boldsymbol{\sigma}(\boldsymbol{u}) : \boldsymbol{\varepsilon}(\boldsymbol{v}) dV = \int_{\partial V} \mathbf{T} \cdot \mathbf{v} dS \tag{4}$$

In this example, we set $\mathbf{T} = \mathbf{0}$. The center of the foot is located at the top/front/left corner of the domain. A no-slip condition is applied to the bottom boundary of the domain, while the front and left faces are constrained to have zero-velocity perpendicular to their faces to satisfy the symmetry of the problem. The part of the top face in contact with the foot is allowed to slip freely, as per the boundary conditions in Sneddon (1946). The other boundaries are allowed to deform freely.

The domain is chosen to be a square prism with edge length 128 times the radius of the foot, and depth 256 times the radius of the foot. Initially, there are 16 and 32 cells in the horizontal and vertical directions. Cells within 128 foot-radii of the center of the foot are then refined (splitting each cell into 8), and then progressive further refinement steps are performed for cells within 64, 32, 16, 8, 4 and 2 foot radii.

References

M. S. Alnæs, J. Blechta, J. Hake, A. Johansson, B. Kehlet, A. Logg, C. Richardson, J. Ring, M. E. Rognes, and G. N. Wells. The fenics project version 1.5. *Archive of Numerical Software*, 3(100), 2015. doi:10.11588/ans.2015.100.20553.

A. Logg, K.-A. Mardal, and G. N. Wells. *Automated solution of differential equations by the finite element method: The FEniCS book*, volume 84. Springer, 2012. ISBN 978-3-642-23098-1. doi:10.1007/978-3-642-23099-8.

I. N. Sneddon. Boussinesq's problem for a flat-ended cylinder. *Proceedings of the Cambridge Philosophical Society*, 42:29, 1946. doi:10.1017/S0305004100022702.